

1 **Estimating radiative forcing with a nonconstant**
2 **feedback parameter and linear response**

3 **Hege-Beate Fredriksen¹, Maria Rugenstein² and Rune Graversen^{1,3}**

4 ¹Department of Physics and Technology, UiT the Arctic University of Norway, Tromsø, Norway

5 ²Colorado State University, Fort Collins, USA

6 ³The Norwegian Meteorological Institute, Norway

7 **Key Points:**

- 8 • We present a new method for estimating radiative forcing and apply it to abrupt4xCO₂,
9 1%CO₂, historical, and future scenario experiments
10 • Including a time-scale dependent feedback parameter results in stronger forcing
11 estimates for the 21st century
12 • The temperature responses to the new forcing are well described by a linear re-
13 sponse

Corresponding author: Hege-Beate Fredriksen, hege-beate.fredriksen@uit.no

Abstract

A new algorithm is proposed for estimating time-evolving global forcing in climate models. The method is a further development of the work of Forster et al. (2013), taking into account the non-constancy of the global feedbacks. We assume that the non-constancy of this global feedback can be explained as a time-scale dependence, associated with linear temperature responses to the forcing on different time scales. With this method we obtain stronger forcing estimates than previously assumed for the representative concentration pathway experiments in the Coupled Model Intercomparison Project Phase 5 (CMIP5). The reason for the higher future forcing is that the global feedback parameter is more negative at shorter time scales than at longer time scales, consistent with the equilibrium climate sensitivity increasing with equilibration time. Our definition of forcing provides a clean separation of forcing and response, and we find that linear temperature response functions estimated from experiments with abrupt quadrupling of CO₂ can be used to predict responses also for future scenarios. In particular, we demonstrate that for most models, the response to our new forcing estimate applied on the 21st century scenarios provides a global surface temperature up to year 2100 consistent with the output of coupled model versions of the respective model.

1 Introduction

Diagnosing the magnitude of a climate forcing is necessary to determine the climate responses to this forcing. However, defining a clear separation between forcing and response is challenging, and no clear distinction exists (Sherwood et al., 2015). In this paper we attempt to apply a separation within a linear temperature response framework, incorporating also the possibility of globally nonconstant atmospheric feedbacks. We test this method on models participating in the Coupled Model Intercomparison Project Phase 5 (CMIP5).

In the most common forcing-feedback framework, the radiative imbalance at the top of the atmosphere (N) is described as

$$N = \lambda T + F, \quad (1)$$

where T is the temperature response, λ is the feedback parameter, and F is the radiative forcing, all evaluated as global means. According to this equation, forcing is the initial radiative imbalance, before the global mean surface temperature starts to respond. However, as discussed by Hansen et al. (2005); Richardson et al. (2019), there are many ways of defining the forcing, allowing various rapid adjustments before diagnosing the radiative imbalance. Forcing estimates are therefore method and model dependent. Some studies even consider multi-annual adjustments associated with ocean inertia (Williams et al., 2008; M. Rugenstein, Gregory, et al., 2016; Menzel & Merlis, 2019). A motivation for this study is therefore to find an estimation method aiming for a clean separation between forcing and response. By design, our method aims at finding the forcing estimates that are the most predictable for the surface temperature responses.

The uncertainties associated with forcing estimates are large, not only due to the different rapid adjustments between models (Smith et al., 2018), but also due to differences in the parameterizations of the radiative transfer (Soden et al., 2018). The instantaneous forcing spread contributes to about half of the total intermodel spread in forcing (Chung & Soden, 2015), and the remaining spread is largely due to fast cloud adjustments (Zelinka et al., 2013). These uncertainties have led to an effort aiming at better characterizing the forcing used for the new CMIP6 model versions (Forster et al., 2016; Pincus et al., 2016). These studies recommend using fixed-SST forcing, largely due to the reduced level of noise by this method as compared to regression-based estimates. Fixed-SST forcing estimates are made by diagnosing the top of atmosphere radiative imbalance after fixing the sea-surface temperatures and letting the atmosphere adjust. These

61 effective forcings include rapid adjustments, e.g. atmospheric temperature and cloud ad-
 62 justments, and are found to be better predictors of global surface temperature responses
 63 than instantaneous forcing estimates (Richardson et al., 2019). There is, however, sub-
 64 substantial land warming in these simulations. Our main motivation is to improve forcing
 65 estimates based on already existing simulations, which can be used for models where fixed-
 66 SST forcing is unavailable, and to circumvent the problem of land warming in fixed-SST
 67 simulations.

In experiments with a time-varying forcing, forcing estimates may be even more uncertain than in idealized experiments with constant forcing. Forster et al. (2013), hereafter F13, computes forcing time series $F(t)$ by rearranging Eq. (1). Their method consists of first determining λ following the regression method of Gregory et al. (2004) using idealized step-forcing simulations, and then using time series of $N(t)$ and $T(t)$ from any experiment to compute what they call adjusted forcing:

$$F(t) = N(t) - \lambda T(t) \quad (2)$$

68 We note that adjusted forcing in F13 does not mean the same as adjusted forcing
 69 in Hansen et al. (2005), where the latter allows only fast stratospheric adjustments to
 70 take place before the forcing is estimated from the top of the atmosphere imbalance in
 71 an idealized step-forcing experiment. Forcing estimates based on regressions in a Gre-
 72 gory plot, such as in Andrews et al. (2012) and F13 are what Forster et al. (2016) refers
 73 to as regression-based methods, assuming a constant feedback parameter.

74 However, several recent studies have pointed out that λ is not a constant (Armour
 75 et al., 2013; Geoffroy, Saint-Martin, Bellon, et al., 2013; Andrews et al., 2015; Gregory
 76 & Andrews, 2016; Proistosescu & Huybers, 2017; M. Rugenstein et al., 2020). Armour
 77 et al. (2013) demonstrate that locally constant feedbacks can result in a globally time-
 78 dependent feedback parameter because the pace of sea surface temperatures (SST) equi-
 79 libration depends on the location, weighting the local feedbacks differently with time.
 80 Other studies demonstrated that also locally, feedbacks change magnitude with equili-
 81 bration time (e.g. Andrews et al., 2015; Andrews & Webb, 2018; M. Rugenstein, Caldeira,
 82 & Knutti, 2016; Proistosescu & Huybers, 2017; Dong et al., 2019, 2020) and also through-
 83 out the historical time period (Paynter & Frölicher, 2015; Gregory & Andrews, 2016; Ar-
 84 mour, 2017; Marvel et al., 2018; Dessler, 2020). The tropical Pacific, the relative warm-
 85 ing of midlatitude or global oceans to the West Pacific warm pool, the North Atlantic,
 86 and the mid- and high latitudes have all been suggested to influence global feedbacks (e.g.
 87 Winton et al., 2010; Trossman et al., 2016; Andrews & Webb, 2018; Dong et al., 2020;
 88 Zelinka et al., 2020). The mechanism most often invoked is the dependence of lower tro-
 89 pospheric stability on the ratio of local and remote SSTs. Regions warming faster than
 90 the West Pacific warm pool ? which sets the temperature of the free troposphere through
 91 deep convection ? show a reduced lower tropospheric stability, a decrease in low-cloud
 92 coverage, and thus, a strong cloud and net radiative effect at the top of the atmosphere
 93 (e.g. Zhou et al., 2016; Ceppi & Gregory, 2017). In the CMIP6 models, the shortwave
 94 cloud feedbacks in the extratropics appear to be more important for the nonconstancy
 95 of λ than clouds in the tropics (Zelinka et al., 2020; Bacmeister et al., 2020), but the rel-
 96 atively short record of global cloud observations makes it difficult to assess cloud mod-
 97 eling against the observations (Loeb et al., 2020). Other studies highlight the dependence
 98 of feedbacks on temperature and radiative forcing (Meraner et al., 2013; Rohrschneider
 99 et al., 2019; Bloch-Johnson et al., 2021).

100 The nonconstancy of λ implies that the forcing definition in Eq. (2) is ambiguous.
 101 This is particularly apparent for strong temperature responses, when λT more strongly
 102 affects the determination of the value of F . Here the magnitude and time-dependence
 103 of λ are particularly important. Larson and Portmann (2016) demonstrated for instance
 104 that λ obtained from regressions in the first 20 yr time period of abrupt4xCO₂ gives higher
 105 forcing estimates compared to regressions in 150 yr time period. This is one of several

106 reasons why Forster et al. (2016) recommends fixed-SST methods instead of regression
107 methods to determine the forcing.

108 We explore how an alternative definition of effective forcing with a time-scale de-
109 pendent λ differs from estimates by F13. To compute these alternative estimates, we de-
110 compose the temperature response assuming it responds linearly to the forcing, and we
111 demonstrate that the linear temperature response to the new forcing is close to the mod-
112 elled temperature response in future scenarios for most CMIP5 models. By a linear re-
113 sponse, we mean the temperature response determined from a linear non-homogeneous
114 system of differential equations, whose solution can be expressed as a convolution be-
115 tween a Green's function and the forcing. Our results suggest that this forcing estimate
116 appears more appropriate for estimating temperature responses using linear response mod-
117 els than previous estimates.

118 Our method is an iterative routine, starting with the F13 estimate of forcing, then
119 computing the linear response to this forcing, which is further used to compute a new
120 forcing estimate, etc., until convergence to a final forcing estimate is obtained. Theory
121 and methods are described in Section 2, and the results are shown in Section 3. In Sec-
122 tion 4, we discuss the assumptions made in our method, and how it compares to other
123 forcing estimates, before we conclude in Section 5.

124 2 Theory and methods

The time-scale dependence of λ is analysed by making use of the same decompo-
sition as in Proistosescu and Huybers (2017), hereafter PH17. While PH17 use the method
to better understand estimates of climate sensitivity, we are interested in the intersect
of the fit with the vertical axis, the initial radiative imbalance. We also estimate param-
eters using a different approach, mainly because our method simplifies the comparison
to methods based on single regression estimates in Gregory plots. The equations that
will be presented in this section provide interpretations of the different λ 's that may ap-
pear in a Gregory plot, as well as interpretations of "forcing estimates" based on regres-
sions on decadal to centennial time scales. The method is based on the assumption that
the temperature response can be decomposed into a sum of K components $T = \sum_{n=1}^K T_n$,
where each component is the exponential temperature response to the forcing on the time
scale τ_n [yrs],

$$T_n(t) = c_n \exp(-t/\tau_n) * F(t). \quad (3)$$

125 The * denotes a convolution, and the factors c_n [$\frac{Km^2}{W}$] are the amplitudes of the tem-
126 perature responses per unit forcing. As further explained in the next subsection, this tem-
127 perature decomposition can be interpreted as either approximating different global-scale
128 processes (such as mixed-layer versus deep ocean responses to forcing) or as regions re-
129 sponding with different pace to the forcing (such as the tropics in general versus regions
130 of upwelling or deep ocean convection). c_n therefore depends on both the feedbacks and
131 thermal inertia associated with different regions, and the fraction of the global area in-
132 volved in the response at time scale τ_n .

Furthermore, the method assumes that constant feedback parameters λ_n exist, with
 $n = 1, \dots, K$ associated with each time scale, such that the terms in Eq. (1) can be de-
composed into the following sums:

$$N(t) = \sum_{n=1}^K N_n(t) = F(t) + \sum_{n=1}^K \lambda_n T_n(t) = F(t) + \lambda(t)T(t) \quad (4)$$

By rewriting Eq. (4), PH17 noted that the time-variation of $\lambda(t)$ can be explained
as a weighted average of the feedbacks associated with different components $T_n(t)$ of the

global temperature:

$$\lambda(t) = \frac{\sum_{n=1}^K \lambda_n T_n(t)}{\sum_{n=1}^K T_n(t)} \quad (5)$$

133 We note that in a 4xCO₂ experiment, we define the forcing to be a constant, and
 134 the slope $\lambda(t)$ must be interpreted as the slope of a line drawn between the fixed forc-
 135 ing F and a point $(T(t), N(t))$. This slope may differ from a linearization around a point
 136 $(T(t), N(t))$ by regressing a range of points (see discussion on feedback definitions in M. A. A. Ru-
 137 genstein and Armour (2021)).

138 Armour et al. (2013) suggested a similar decomposition, but interpreted the com-
 139 ponents as locally constant feedbacks multiplied by local temperatures with different time
 140 evolution. However, recent studies suggest that non-local feedbacks are also important
 141 (Andrews et al., 2015; Zhou et al., 2016; Dong et al., 2019; Bloch-Johnson et al., 2020),
 142 meaning that temperature changes in one region, and in particular the West Pacific, can
 143 influence feedbacks globally.

144 2.1 Linear model and response

A simple model of temperature changes in the climate system can be constructed
 by considering different boxes or components that store and exchange energy. If assum-
 ing that all anomalous heat fluxes are linearly related to temperature anomalies in the
 system, the heat uptake in all boxes can be written into a linear non-homogeneous sys-
 tem

$$\mathbf{C} \frac{d\mathbf{T}(t)}{dt} = \mathbf{K}\mathbf{T}(t) + \mathbf{F}(t) \quad (6)$$

145 By choosing the vector of temperature change components \mathbf{T} to be K -dimensional,
 146 the system describes K components that will respond on K different time scales, and
 147 the vector \mathbf{F} the atmospheric forcing acting directly on each component. The vector \mathbf{F}
 148 could in principle contain different forcings in different regions. The heat capacities [$\frac{W_{yr}}{m^2 K}$]
 149 associated with each component are along the diagonal of the diagonal $K \times K$ matrix
 150 \mathbf{C} , and coefficients for heat exchange between components and heat loss to the atmo-
 151 sphere [$\frac{W}{m^2 K}$] constitute the matrix \mathbf{K} . The left-hand side of this equation describes the
 152 heat uptake of each component, and the sum of all heat uptakes must equal the net ra-
 153 diative imbalance N . In this sum of all components, all fluxes between components cancel
 154 out, and the sum reduces to Eq. (4).

155 Linear systems like this have been widely studied, often using one, two or three boxes
 156 (e.g. Geoffroy, Saint-Martin, Olivié, et al., 2013; Fredriksen & Rypdal, 2017). Symmet-
 157 ric matrices \mathbf{K} will describe diffusive heat fluxes depending on the temperature differ-
 158 ence between two boxes, and feedback parameters will appear on its diagonal. Non-symmetric
 159 parts may be due to the dependence of temperature anomalies in one box only. For in-
 160 stance change in sinking processes due to temperature anomalies in the North Atlantic
 161 regarded as one box, may by mass continuity induce horizontal mass and hence energy
 162 fluxes from adjacent ocean basins regarded as other boxes, independent of the temper-
 163 ature change in these boxes. \mathbf{K} may also incorporate heat fluxes to the deep ocean if as-
 164 suming they can be modelled as linear functions of temperature components (e.g. Held
 165 et al., 2010; Geoffroy, Saint-Martin, Olivié, et al., 2013).

By applying the method variation of parameters, it can be shown that the solu-
 tion to Eq. (6) is (see the supporting information):

$$\mathbf{T}(t) = \int_{-\infty}^t e^{(t-s)\mathbf{C}^{-1}\mathbf{K}} \mathbf{C}^{-1}\mathbf{F}(s) ds, \quad (7)$$

showing that the temperature at time t is a response to the forcing experienced at all
 previous times s . If the matrix $\mathbf{C}^{-1}\mathbf{K}$ has only negative eigenvalues, $-1/\tau_n$, the solu-

tion for each temperature component $T_k(t)$ will be a weighted sum of K exponential responses to the global average forcing F with time scales τ_n (where the weights β_n are determined by eigenvalues, eigenvectors, and heat capacities),

$$T_k(t) = \int_{-\infty}^t \sum_{n=1}^K \beta_n e^{(s-t)/\tau_n} F(s) ds \quad (8)$$

Furthermore, the global surface temperature is a weighted average of the components $T_k(t)$:

$$\overline{T}(t) = \sum_{n=1}^K c_n \int_{-\infty}^t e^{(s-t)/\tau_n} F(s) ds \quad (9)$$

166 where we define the new weights c_n to be an area-weighted average of the weights β_n .
 167 If the forcing is not the same in all regions, Eq. (9) is still valid if the regional forcings
 168 are scaled versions of the global average forcing. We recognize Eq. (9) as a convolution
 169 between a Green's function $G(t)$ and a forcing $F(t)$, consistent with Eq. (3): $T(t) = G(t) * F(t)$
 170 $F(t) = \int_{-\infty}^t G(t-s)F(s)ds$, with $G(t) = \sum_{n=1}^K G_n(t) = \sum_{n=1}^K c_n \exp(-t/\tau_n)$, assum-
 171 ing negative eigenvalues.

172 2.2 Estimating linear response in abrupt 4xCO₂ experiments

173 To simplify the estimation of parameters of these responses (time scales τ_n and am-
 174 plitudes c_n), we start by fixing the time scales, such that T and N depend linearly on
 175 the remaining parameters c_n . We find that the exact choice of time scales is not impor-
 176 tant, as long as we choose them well separated, and within the range of expected time
 177 scales. Annual time scales are important over land and shallow ocean areas, while decadal
 178 and centennial time scales are particularly important in ocean regions with mixing to
 179 the deeper oceans, and hence higher thermal inertia. Following PH17, we use three dif-
 180 ferent time scales. They find three time scales to be the smallest number that well de-
 181 scribes the temperature responses. In addition as explained later, we will assume the ex-
 182 istence of a fourth time scale explaining slower temperature responses than can be ob-
 183 served in the records studied in this paper.

184 We analyse data from 21 CMIP5 models, available at [https://esgf-node.llnl](https://esgf-node.llnl.gov/projects/cmip5/)
 185 [.gov/projects/cmip5/](https://esgf-node.llnl.gov/projects/cmip5/). The variables used are global annual averages of surface air tem-
 186 peratures (tas), and net top-of-atmosphere radiation, computed as the difference between
 187 incoming shortwave radiation and outgoing longwave and shortwave radiation (rsdt - rlt
 188 - rsut). To minimize the effect of possible model drifts, the temperature $T(t)$ and the
 189 variables used to compute the net top of atmosphere radiation $N(t)$ time series are de-
 190 fined as deviations from linear trends in the corresponding time period of the control run
 191 (trend values for the abrupt4xCO₂ period are given in Table S1, and are very small). With
 192 this definition we also avoid non-zero means of $N(t)$ in equilibrium, which is the case for
 193 many models (Forster et al., 2013).

194 The shortest time scale τ_1 is chosen to be a random number between 1 and 6 years,
 195 the second time scale τ_2 is a random factor between 5 and 10 multiplied by τ_1 , and the
 196 third is a randomly chosen time scale between 80 and 1000 years. The random choice
 197 is done 1000 times for each model, and finally, for each model, we keep the set of τ_n with
 198 the best (least squares) fit to the modelled temperature evolution for 150 years after an
 199 abrupt quadrupling of CO₂. The resulting parameters are dependent on the length of
 200 the time series used. If using longer time series the longest time-scale responses may change
 201 the most, but these are also the least important for our 21st century analyses.

The temperature response for these step-forcing experiments can be found by com-
 puting the integrals in Eq. (9) with a constant forcing F_{4xCO_2} for $t > 0$. This integral

results in

$$T_{4xCO_2}(t) = \sum_{n=1}^K a_n (1 - e^{-t/\tau_n}) \quad (10)$$

where $a_n = c_n \tau_n F_{4xCO_2}$ is the equilibrium temperature of each component, and the equilibrium climate sensitivity (ECS) is defined as $\frac{1}{2} \sum_{n=1}^K a_n$ (equilibrium response to a doubling of CO_2).

The expression for N is derived as:

$$\begin{aligned} N_{4xCO_2}(t) &= F_{4xCO_2} + \sum_{n=1}^K (\lambda_n T_n(t)) \\ &= F_{4xCO_2} + \sum_{n=1}^K (\lambda_n a_n (1 - e^{-t/\tau_n})) \\ &= F_{4xCO_2} + \sum_{n=1}^K \lambda_n a_n - \sum_{n=1}^K \lambda_n a_n e^{-t/\tau_n} \\ &= - \sum_{n=1}^K \lambda_n a_n e^{-t/\tau_n} \end{aligned}$$

where we in the last step set that $F_{4xCO_2} + \sum_{n=1}^K \lambda_n a_n = 0$, due to the constraint that $N \rightarrow 0$ when $t \rightarrow \infty$. Introducing the notation that $b_n = -a_n \lambda_n$ gives us $N_{4xCO_2}(t) = \sum_{n=1}^K N_n(t) = \sum_{n=1}^K b_n e^{-t/\tau_n}$, and $F_{4xCO_2} = - \sum_{n=1}^K \lambda_n a_n = \sum_{n=1}^K b_n$.

The parameters a_n, b_n could be found using linear regression, but that does sometimes violate the physical assumption that these should have the same sign as the forcing. Therefore we have used the non-negative least squares algorithm to ensure positive parameters. This is used only for finding a_n , and the resulting temperature responses are shown in Figure 1 b). This method could in principle also have been used to find b_n , but this does not seem to provide a sufficiently good fit on the short scales. Instead, λ_n are determined in a Gregory plot, and then used to compute $b_n = -\lambda_n a_n$.

2.3 Algorithm for estimating λ_n

The $\lambda_n, n = 1, \dots, K$ are all determined from linear fits in a Gregory plot, as shown in Figure 1 a). We start with estimating λ_3 corresponding to time scale τ_3 , then we estimate λ_2 , and finally λ_1 . We assume that the sum $\sum_{n=1}^3 a_n$ underestimates the equilibrium response, since the sum excludes the response on the multi-millennial scale τ_4 . However, we assume τ_4 is so large that we can make the following approximations for $t \leq 150$ years:

$$T_4(t) = a_4 (1 - e^{-t/\tau_4}) \approx 0 \quad (11)$$

$$N_4(t) = b_4 e^{-t/\tau_4} \approx b_4 \quad (12)$$

Hence $T(t) \approx \sum_{n=1}^3 T_n(t)$ and $N(t) \approx b_4 + \sum_{n=1}^3 N_n(t)$, where b_4 could be interpreted as a constant heat flux going into the deeper oceans, hereby not leading to surface warming on short time scales. We made the somewhat arbitrary choice of setting $\tau_4 = 5000$ years, and assume $\lambda_4 = \lambda_3$. The results are not sensitive to the choice of τ_4 as long as the approximations in Eqs. (11) and (12) hold. In the 150 year long runs considered in this paper, we have no information about λ_4 , but longer runs show that the feedback parameter changes little on the longer time scales (M. Rugenstein et al., 2020).

Determining λ_3 : We consider only temperatures larger than the equilibrium temperature of the first two components, such that $T_1(t) + T_2(t) \approx a_1 + a_2$, and we have: $N(t) \approx -\lambda_3(a_3 - T_3(t)) + b_4$. The total temperature is therefore approximated by $T(t) \approx$

233 $a_1 + a_2 + T_3(t)$, resulting in $N(t) \approx -\lambda_3(a_1 + a_2 + a_3 - T(t)) + b_4$. This shows that N is
 234 approximately a linear function of T with slope λ_3 for $T > a_1 + a_2$. Therefore, λ_3 is
 235 computed by linear regression of these points, and the equilibrium temperature found
 236 by following this line until $N = 0$. This equilibrium estimate should be higher than $\sum_{n=1}^3 a_n$,
 237 and the difference is a_4 . Whenever the unphysical result $a_4 < 0$ is obtained, we exclude
 238 the chosen time scales from our analysis.

239 **Determining λ_2 :** First we subtract our estimates of $T_3(t)$, $T_4(t)$ and $N_3(t)$, $N_4(t)$
 240 from the time series $T(t)$ and $N(t)$, respectively. We then obtain estimates of $T_1(t) +$
 241 $T_2(t)$ and $N_1(t) + N_2(t)$, and these points are the dark gray dots in Figure 1a). For $a_1 <$
 242 $T_1(t) + T_2(t) < a_1 + a_2$, $T_1(t) + T_2(t)$ is approximately $a_1 + T_2(t)$, and should equal
 243 the equilibrium value $a_1 + a_2$ when $N_1(t) + N_2(t) = 0$. In this range, $N_1(t) + N_2(t) \approx$
 244 $-\lambda_2(a_2 - T_2(t))$, approximately linearly related to $T_1(t) + T_2(t)$. Therefore, λ_2 is esti-
 245 mated using a least-squares algorithm forcing the linear fit to go through the point $(a_1 +$
 246 $a_2, 0)$.

247 **Determining λ_1 :** We subtract estimates of $(T_2(t), N_2(t))$ from the dark gray dots
 248 to obtain estimates of $T_1(t)$ and $N_1(t)$ (light gray dots in Figure 1). We have now $N_1(t) \approx$
 249 $-\lambda_1(a_1 - T_1(t))$, and we can, as previously, use least squares to compute λ_1 , forcing the
 250 linear fit to pass the point $(a_1, 0)$.

251 In the least squares fits, we also include an upper time limit to the set of points
 252 to be included in the calculation. This limit is set to the first time step after reaching
 253 99% of the equilibrium temperature of the component of interest. In this way, our slope
 254 is associated with the response on the particular time scale τ_n , and little influenced by
 255 the fluctuations around the equilibrium values. Changing this limit to e.g. 90% or 95%
 256 has only minor effects on the results. Feedback parameters associated with fluctuations
 257 around the base state, or more precisely, radiative restoring coefficients are studied in
 258 several papers (Colman & Power, 2010; Colman & Hanson, 2013; Lutsko & Takahashi,
 259 2018; Bloch-Johnson et al., 2020). Depending on the model, they can be similar or dif-
 260 ferent from those associated with the final fluctuation after a quadrupling of CO_2 (M. Ru-
 261 genstein et al., 2020), and they may also differ from feedbacks associated with forced re-
 262 sponses (e.g. Zhou et al., 2015; Dessler & Forster, 2018).

263 When all a_n , λ_n are estimated, we compute $b_n = -\lambda_n a_n$ and we finally have our
 264 estimate of $F_{4\times\text{CO}_2} = \sum_{n=1}^4 b_n$. That is, the sum of the initial radiative imbalance of
 265 all 4 components.

266 2.4 New estimates of effective forcing time series

267 Using our parameter estimates from the previous subsections, we can for any exper-
 268 iment use the global mean evolutions of $T(t)$ and $N(t)$ to compute a new estimate
 269 of the effective forcing as follows:

- 270 1. Compute $F(t)$ using F13's method (a single estimate of λ), and take this as the
 271 initial estimate of the effective forcing.
- 272 2. Use this forcing estimate and amplitudes $c_n = \frac{a_n}{\tau_n F_{4\times\text{CO}_2}}$ estimated from $4\times\text{CO}_2$
 273 experiments to compute the components $T_n(t)$ from Eq. (3) by performing con-
 274 volution integrals.
- 275 3. A new estimate of $F(t)$ can then be computed as:

$$F(t) = N(t) - \sum_n \lambda_n T_n(t) \quad (13)$$

- 276 4. Repeat steps 2-3 until convergence of $F(t)$. We have used 20 iterations.

277 We demonstrate how the method can be applied to study the forcing for 1% CO_2
 278 experiments, the historical period and the four representative concentration pathways
 (RCPs) RCP2.6, RCP4.5, RCP6.0 and RCP8.5.

Table 1. Estimated parameters, where we define F_{2x} and T_{2x} to be half the forcing and equilibrium temperature estimated for a quadrupling of CO_2 . The parameters in parentheses $(-\lambda)$, (F_{2x}) and (T_{2x}) are estimated from a single linear regression over years 1-150 in a Gregory plot. The results differ slightly from the numbers reported from the Gregory method by Andrews et al. (2012), possibly because of minor differences in the way global annual average values are constructed. For one model (GFDL-ESM2G) the best fit consists of two exponential responses, where we estimate $a_2 = 0$ and report $\lambda_2 = b_2/a_2$ as 'NaN'.

	τ_1	τ_2	τ_3	$-\lambda_1$	$-\lambda_2$	$-\lambda_3$	$(-\lambda)$	F_{2x}	(F_{2x})	T_{2x}	(T_{2x})
ACCESS1-0	2.43	12.79	231.10	1.30	1.12	0.56	0.78	3.72	2.97	4.33	3.83
ACCESS1-3	1.13	5.80	150.10	1.46	1.30	0.56	0.82	3.60	2.89	4.12	3.53
CanESM2	2.86	26.39	279.11	1.30	1.01	0.91	1.04	4.24	3.83	3.83	3.69
CCSM4	1.04	5.52	197.28	1.32	1.77	0.90	1.18	4.02	3.47	3.19	2.94
CNRM-CM5	1.45	10.71	392.15	1.38	1.09	1.22	1.14	3.87	3.71	3.20	3.25
CSIRO-Mk3-6-0	1.62	11.29	308.98	1.86	1.12	0.41	0.63	3.94	2.58	4.94	4.08
GFDL-CM3	3.28	32.58	98.81	1.21	0.80	0.63	0.75	3.61	2.99	4.24	3.97
GFDL-ESM2G	2.98	17.50	291.97	1.76	NaN	0.90	1.29	3.65	3.09	2.67	2.39
GFDL-ESM2M	1.03	5.77	240.02	1.52	1.58	1.22	1.38	3.58	3.36	2.52	2.44
GISS-E2-H	1.56	10.43	186.27	2.02	1.83	1.40	1.65	4.21	3.81	2.39	2.31
GISS-E2-R	1.51	10.61	232.40	2.98	1.02	1.42	1.79	5.09	3.78	2.25	2.11
HadGEM2-ES	1.01	8.39	367.62	1.96	0.89	0.35	0.63	4.02	2.90	5.91	4.61
inmcm4	1.02	5.65	597.43	1.90	1.48	1.28	1.43	3.18	2.98	2.14	2.08
IPSL-CM5A-LR	1.72	16.54	163.83	1.03	0.84	0.58	0.75	3.43	3.10	4.55	4.13
IPSL-CM5B-LR	1.21	8.01	80.30	2.39	1.11	0.91	1.02	3.64	2.64	2.68	2.60
MIROC-ESM	1.78	11.32	266.35	1.96	0.92	0.68	0.91	5.37	4.26	5.21	4.67
MIROC5	2.77	15.17	89.28	1.72	1.43	1.36	1.52	4.38	4.13	2.80	2.72
MPI-ESM-LR	1.81	9.20	202.56	1.30	1.50	0.86	1.13	4.53	4.09	3.91	3.63
MPI-ESM-MR	1.02	6.23	158.54	2.27	1.45	0.94	1.18	5.15	4.07	3.67	3.46
MRI-CGCM3	1.42	11.61	233.73	2.22	1.34	0.96	1.25	4.05	3.24	2.76	2.60
NorESM1-M	1.75	9.34	273.12	1.87	1.52	0.78	1.11	3.88	3.10	3.17	2.80
Model mean	1.73	11.73	231.26	1.73	1.28	0.90	1.12	4.04	3.38	3.50	3.20
Standard deviation	0.69	6.58	115.35	0.45	0.30	0.31	0.31	0.56	0.50	1.02	0.78

279 3 Results

280 The results of the linear response fit for $T(t)$ and $N(t)$ following an abrupt qua-
281 drupling of CO_2 are given for the model NorESM1-M in Figure 1, and the estimated pa-
282 rameters are listed in Table 1. We note from Figure 1a) that both the forcing and equi-
283 librium temperature estimates are higher than when obtained from a straight line fit.
284 The narrow spread of the light blue lines also indicate that the choice of time scales is
285 of little importance, and hence not affecting the overall conclusions. Similar plots are
286 shown for the other models listed in Table 1 in the Supporting information. The uncer-
287 tainty in both the forcing estimate and ECS estimate vary substantially from model to
288 model. Models with a rapid initial warming, such as GISS-E2-R, have fewer points con-
289 straining the regression estimate for the shortest time scale, implying larger uncertainty
290 of the forcing.

291 An overview of all our estimates of the $4x\text{CO}_2$ forcing is presented in Figure 2. In
292 addition, we compare our forcing estimates to regression estimates done for years 1-20
293 and years 1-150. In all except one model, the 1-20 year regression gives a higher estimate

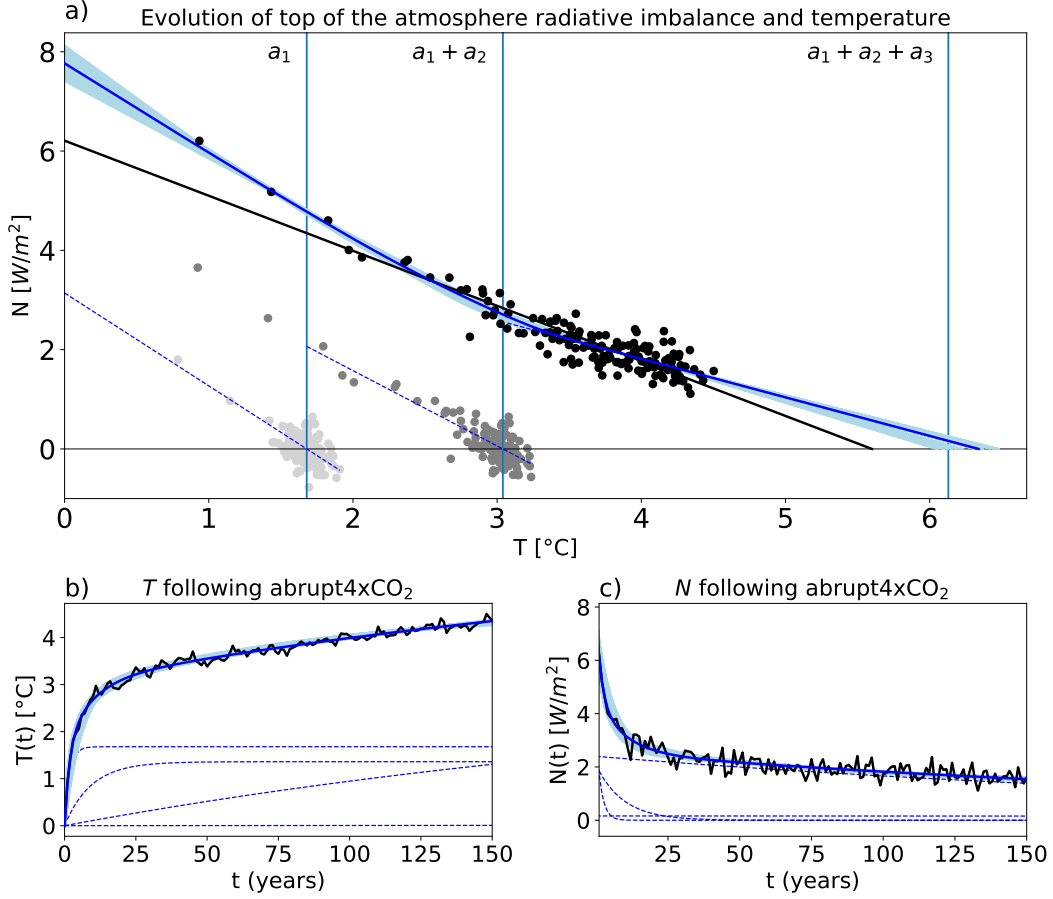


Figure 1. Results for NorESM1-M: a) The black dots and line is a conventional Gregory plot, the light blue lines (recognized as light-blue shading) are our fits to the black points with 1000 different choices of time scales, and the dark blue fit is when using the best (least squares) fits for the temperature in b). Vertical blue lines are the sums of equilibrium temperatures $\sum_{n=1}^m a_n$, $m = 1, 2, 3$. The dark (light) gray dots are N vs. T after subtracting components associated with the third (and second) time scales, and the dashed blue lines are fits to these dots. b) The black curve is the climate model temperature output, and the light blue curves are best fits to the modelled temperature using 1000 different choices of time scales. The dark blue curve is the best fit, and the dashed blue curves are the individual components due to the four time scales which are summed to obtain this fit. c) As panel b), but for the change in net top of the atmosphere radiation.

294 than the 1-150 year regression. And in all but two models, our best forcing estimate is
 295 even higher than estimates obtained from regression of years 1-20. The fixed-SST 4xCO₂
 296 forcing estimates reported by Andrews et al. (2012) are higher than regression-based es-
 297 timates over 150 years for most of the models where this is available, but smaller than
 298 our new forcing estimates.

299 Using global annual means of $N(t)$ and $T(t)$ from the coupled models, we continue
 300 by testing the algorithm described in Section 2.4 for 1% CO₂ experiments. In these ex-
 301 periments we expect a linearly increasing forcing, because to first order, for small increases
 302 in CO₂ the forcing depends logarithmically on the CO₂ concentration (Myhre et al., 1998)

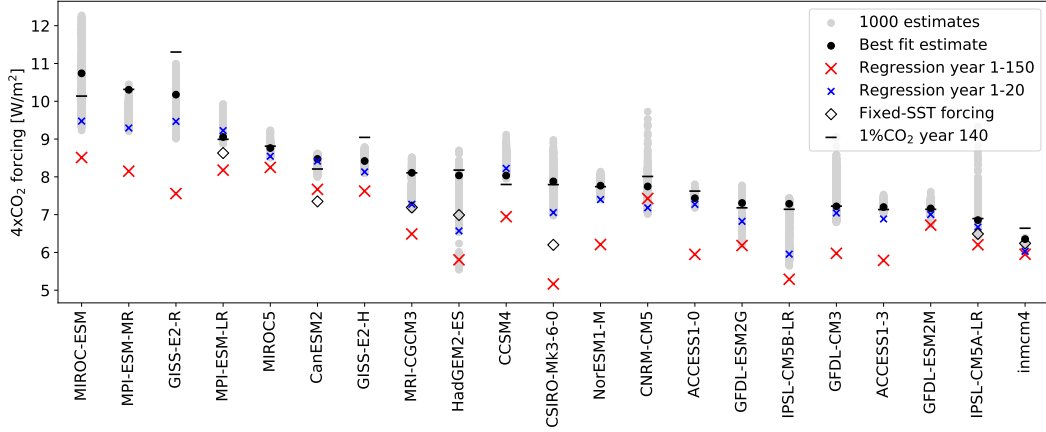


Figure 2. A summary of the $4xCO_2$ forcing estimates made in this paper, to provide an overview of their uncertainties and how they compare to regression estimates. The $1\%CO_2$ estimates are the linear fits to the estimated $1\% CO_2$ forcing time series evaluated in year 140, the time of quadrupling (except for the models GFDL-ESM2G and GFDL-ESM2M, where the estimates are instead twice the doubling estimates in year 70). Fixed-SST estimates are taken from Andrews et al. (2012) for the models where these are available.

(see limitations of this discussed in Byrne and Goldblatt (2014); Etminan et al. (2016); Gregory et al. (2015); Bloch-Johnson et al. (2021)). A linear increase is indeed what we observe for NorESM1-M in Figure 3, for both the initial and the new forcing estimate. For the new estimate we note a high consistency between the climate model temperature output and the linear response to the forcing. This result suggests that our method can successfully construct forcing estimates that well predicts the surface temperature responses. Results for other models are similar, and are shown in the supporting information. After 140 years of 1% increase the CO_2 concentration is quadrupled, and the linear fit to the $1\% CO_2$ forcing time series evaluated in year 140 is yet another estimate of F_{4xCO_2} , which we include in Figure 2. For most models this estimate is close to our best estimates determined from abrupt $4xCO_2$ experiments.

Next we apply the algorithm to the historical and RCP experiments to compute forcing estimates for the time period 1850 - 2100. Our new forcing estimate for the historical and RCP8.5 experiment for NorESM1-M diverges from the forcing estimate using a single feedback parameter when approaching the end of the 21st century (Figure 4a). The difference is about $2 W/m^2$ in 2100, and smaller differences are seen during the historical period. As a result, the sum of the linear temperature responses we compute by convolving with the two forcing estimates according to Eq. (3) also diverge (dashed curves in Figure 4b), reaching a difference of almost 1 degree in year 2100. We note that the linear response to our new forcing (dashed blue curve) is remarkably close to the climate model temperature output, indicating that our alternative forcing definition and linear response assumption is the better approximation for this model. This result holds also for the other RCP scenarios (see Figures S109 - S111 in the supporting information).

By computing the time-varying feedback parameter $\lambda(t)$ using Eq. (5), we find a generally higher magnitude than the single estimate of λ . During the historical period the global temperature response is often close to 0, causing high fluctuations in the estimated $\lambda(t)$. The estimate becomes more stable for the future scenarios, where we find a slowly decreasing magnitude of $\lambda(t)$, consistent with a higher weighting of the slow responses. For all years in the experiment, the magnitude of $\lambda(t)$ is still considerably higher

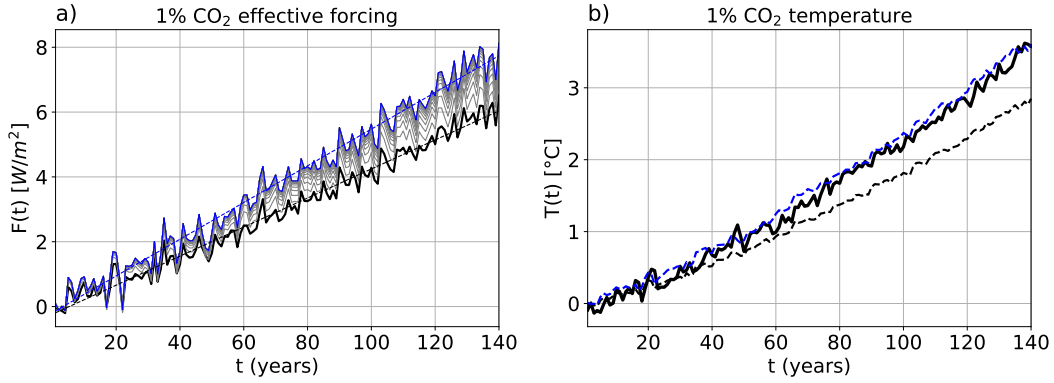


Figure 3. Results for NorESM1-M: a) The black curve is the forcing computed as in F13, using a single and constant value of λ . The gray curves are the iterations of the algorithm described in section 2.4, using three different λ 's, and the blue curve the new forcing obtained by convergence after 20 iterations. The dashed lines are linear fits to the initial and final forcing estimates. b) The thick black curve is the modelled temperature change, and the black and blue dashed curves the linear responses to the black and blue curves in a), applying the same response function as estimated in Figure 1 b).

332 than the single regression estimate, hence the term $-\lambda(t)T(t)$ gives a higher contribu-
 333 tion to the forcing estimate. This effect on the forcing is however only visible when the
 334 temperature response is strong.

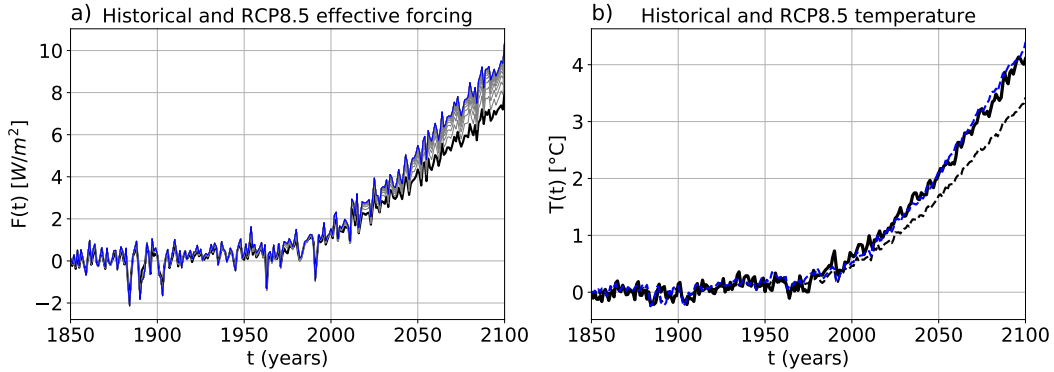


Figure 4. Similar to Figure 3, but for NorESM1-M historical and RCP8.5 experiment.

335 Repeating the analysis in Figure 4 for all models and RCP scenarios shows that
 336 the method presented here works well for many models, but not all (Figures in support-
 337 ing information). A summary of these results are given in Figure 5, where panel a)
 338 compares the mean estimated forcing over years 2091-2100 using the two different
 339 methods. The names of the scenarios are constructed to reflect the intended forcing in the end of
 340 the 21st century (van Vuuren et al., 2011), and these forcing levels are also shown for
 341 comparison. We find that model estimates using F13's method are centered at lower val-
 342 ues, while our new forcing estimates are centered close to or slightly above the intended
 343 levels. However, the intended forcing is difficult to prescribe as it depends on model-specific
 344 fast adjustments, so we can only expect these to be approximate values. The GISS-E2-

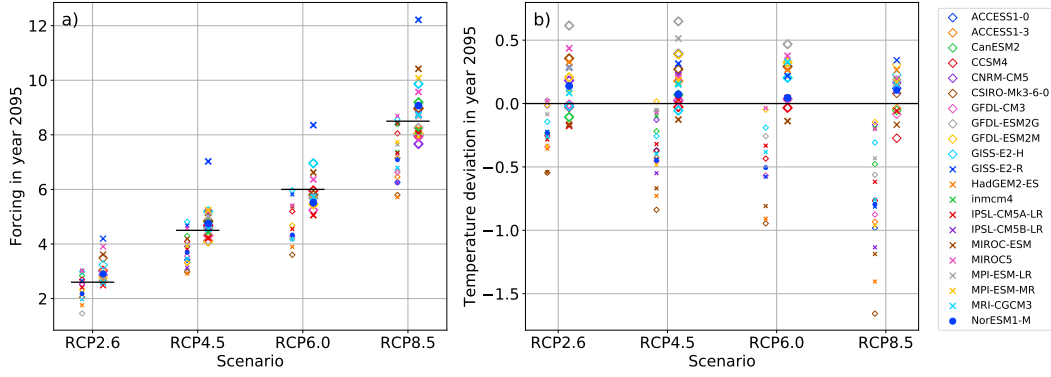


Figure 5. Estimated year 2095 forcing (a) and temperature difference between the result of the linear response and the climate model output (b). For each scenario, the left points show results using F13’s method, and the right points show results using our method. Values in year 2095 are computed by averaging over the ten years 2091-2100. The forcing levels 2.6, 4.5, 6.0 and 8.5 W/m² are also shown for reference in a) as horizontal black lines.

345 R model might be considered as an outlier, and its response to abrupt4xCO₂ is also visu-
 346 ally different from the other models.

347 Consistent with the increase in forcing level, we observe an increase in the estimated
 348 linear temperature responses in panel b). The linear responses to F13 forcing are mostly
 349 lower than the climate model temperature output, and the responses to our new forc-
 350 ing are scattered around, with a center slightly above. Some deviation from the climate
 351 model temperature is expected due to internal variability, and to assess this expected
 352 uncertainty, we refer to the model spread of the Community Earth System Model Large
 353 Ensemble (CESM-LE) (Kay et al., 2015). Here 40 model simulations for the historical
 354 + RCP8.5 scenarios from the same model show a model spread of around 0.4 K, which
 355 is attributed to internal variability.

356 Using F13 forcing, the linear response is within these uncertainties for only a few
 357 models. For the new forcing, more models are within this uncertainty range than out-
 358 side. There are also other uncertainties to consider, e.g. associated with our parameter
 359 estimation method, probably making the expected uncertainty interval larger than 0.4
 360 K. The uncertainty due to internal variability is also model-dependent (Olonscheck et
 361 al., 2020), hence it is difficult to identify models where our linear response hypoth-
 362 esis and forcing estimation method fail.

363 We note also that the uncertainty of the future scenario forcing estimates is strongly
 364 related to the uncertainty of the 4xCO₂ forcing, since both are highly influenced by λ₁
 365 (the inter-model correlation between our 4xCO₂ and RCP8.5 forcing is 0.82). This is par-
 366 ticularly apparent for the GISS-E2-R model, where the response of the first few years
 367 is so abrupt that forcing estimates, and hence linear responses, are uncertain with both
 368 our and F13’s estimation method.

369 In the two models CNRM-CM5 and MIROC5 the two forcing estimates are very
 370 similar, because the feedback is close to constant for all years. For these models we find
 371 also that the forcing estimate based on a single feedback parameter gives a slightly bet-
 372 ter estimate of the linear response. So if the global feedback in fact is constant for all
 373 years considered here, using all years in the regression should give a more certain esti-
 374 mate of the feedback parameter, and therefore also more certain forcing estimates.

375 For the three models GFDL-ESM2G, GFDL-ESM2M, and inmcm4 we find that
 376 our method is performing less well (see Figures in the Supporting information). The rea-
 377 son is probably linked to the almost constant $4xCO_2$ temperature responses over years
 378 $\sim 20 - 70$, $\sim 20 - 60$ and $\sim 20 - 120$, respectively. Our linear response with exponen-
 379 tially relaxing temperatures always predicts continuously increasing temperatures, which
 380 therefore poorly approximates these $4xCO_2$ global temperatures. The flattening of the
 381 response could possibly be linked to changes in the ocean circulation, e.g. a slowdown
 382 of the Atlantic meridional overturning circulation. In that case, linear systems with com-
 383 plex eigenvalues giving oscillatory responses could be an alternative solution. Hence, we
 384 will not disregard linear response in these results, but leave further testing of including
 385 oscillations in the responses to future studies.

386 4 Discussion

387 For most abrupt $4xCO_2$ experiments the Gregory plot follows a convex curve, hence
 388 our forcing estimates are mostly higher than those found from simple regression anal-
 389 yses over 150 years (Andrews et al., 2012), or using only the first 20 years (Andrews et
 390 al., 2015; Larson & Portmann, 2016). As suggested by PH17, this convexity could be ex-
 391 plained by considering different feedback parameters associated with the different time
 392 scales of the responses. The time-scale dependence of the feedback parameter could be
 393 due to feedbacks varying in strength at different time scales, or it could be regionally dif-
 394 ferent feedbacks weighted differently with time in the global average when the pattern
 395 of surface warming evolves. Since it is likely a combination of these circumstances, an
 396 interpretation of our parameters could be summarized into: λ_1 : Average of annual-scale
 397 feedbacks in regions with strong annual-scale responses, λ_2 : Average of decadal-scale feed-
 398 backs in regions with strong decadal-scale responses, λ_3 : Average of centennial-scale feed-
 399 backs in regions with strong centennial-scale responses. Or as we come back to later, this
 400 description could also be considered an approximation of feedbacks changing with cli-
 401 mate state.

402 The fixed-SST estimation method does not include time-variation and uncertain-
 403 ties in the feedback parameter. Instead, extra model simulations are made with SSTs
 404 fixed to climatological values, and the top of atmosphere radiative imbalance is diagnosed.
 405 A drawback of this method is that atmospheric and land surface temperatures are al-
 406 lowed to change. Hence the global temperature anomaly is not 0 when the radiative im-
 407 balance is diagnosed, and the forcing estimate is therefore contaminated with fast feed-
 408 back processes associated with land warming. The fixed-SST estimates should be more
 409 comparable to our radiative imbalance after some months of adjustments of $T(t)$ and $N(t)$,
 410 and Figure 2 shows that they are indeed lower than our estimates for the models where
 411 they are available.

412 Ideally the fixed-SST method should be extended to fix the land surface temper-
 413 atures also, in order to provide a consistent framework where forcing and feedbacks are
 414 well separated. Due to technical difficulties, this has only been done for one complex global
 415 climate model so far (Andrews et al., 2021). As discussed by Andrews et al. (2021), sev-
 416 eral methods have been suggested to correct fixed-SST estimates to account for effects
 417 of land temperature changes. One could for instance extrapolate the estimate to $T =$
 418 0 using Eq. (2) given that we know the feedback parameter, or use radiative kernels (Richardson
 419 et al., 2019). Richardson et al. (2019) call these estimates Adjusted Effective radiative
 420 forcing, and find also these to be the best predictors for global surface temperatures be-
 421 cause they have the efficacies closest to 1.

422 Efficacy factors are introduced to correct for differences in how strong the climate
 423 response is to different forcing agents, due to e.g. differences in rapid adjustments, or ef-
 424 fects of a forcing being concentrated in certain regions. Forcing in experiments consid-
 425 ered in this study are dominated by CO_2 , a well-mixed greenhouse gas. Other forcings

426 present during the historical period and future scenarios could be more spatially inho-
 427 mogeneous, e.g. aerosols, and contribute to different spatial patterns of the response. We
 428 neglect this effect when applying the parameters estimated for abrupt4xCO₂ experiments
 429 to other experiments, and assume the regional patterns to evolve similarly for different
 430 experiments. During the historical period, a changing feedback parameter will only re-
 431 sult in weak changes in our forcing estimate since the temperature responses are still rel-
 432 atively weak. But if applying our method to strong forcings other than CO₂, the pos-
 433 sible effect of efficacies should be investigated first.

434 When estimating a time-varying forcing, an alternative to fixing the SSTs to cli-
 435 matological values (as employed in RFMIP) is to prescribe the SSTs to e.g. the simu-
 436 lated historical values from the coupled model (as employed in AerChemMIP). These
 437 methods produce relatively similar results (Forster et al., 2016), and will both have a lower
 438 uncertainty than regression-based estimates. Regression-based estimates are influenced
 439 by changes in $T(t)$ arising due to internal variability, e.g. El Niño events, which could
 440 drive changes in $N(t)$. In prescribed-SST methods the temperature-driven changes in
 441 $N(t)$ is subtracted, resulting in a reduced noise level in the forcing estimate (Forster et
 442 al., 2013).

443 The theory described in this paper does not include an explicit temperature-dependence
 444 of the feedback parameter (Rohrshneider et al., 2019; Bloch-Johnson et al., 2021), since
 445 it is assumed that Eq. (6) is linear and \mathbf{K} is independent of temperature. However, our
 446 estimation algorithm does not clearly distinguish between a time-scale dependence and
 447 a temperature-dependence of the feedbacks, since these dependencies are intrinsically linked.
 448 In particular, the strong temperature responses to 4xCO₂ is invoked on the long time
 449 scales, where the responses to the shorter time scales have already been realised, hereby
 450 affecting the feedback parameters if they have temperature dependence. If the 4xCO₂
 451 responses have temperature-dependent feedbacks, the model needed to explicitly explain
 452 them becomes nonlinear, and our linear approach may perform less well in providing re-
 453 sponses to other scenarios with weaker or stronger temperature responses than that of
 454 4xCO₂. We believe this only causes smaller errors in the temperature responses stud-
 455 ied here, but it is a potential explanation for our forcing and responses for the future sce-
 456 narios being slightly overestimated.

457 Linear response theory is widely used to describe responses of climate variables.
 458 If a forcing record is known, linear response is a computationally cheap tool to estimate
 459 e.g. temperature responses compared to running a fully coupled climate model. Many
 460 studies assume a Green’s function taking a certain form, with unknown parameters that
 461 need to be estimated. For box models taking the form of Eq. (6) the Green’s function
 462 is a sum of exponential functions, but power-laws with fewer parameters have also been
 463 used with success (Rypdal & Rypdal, 2014; Fredriksen & Rypdal, 2017). Linear responses
 464 to RCP forcing are often studied using a non-parametric approach developed by Good
 465 et al. (2011). In the supporting information we show how this method relates to our lin-
 466 ear model. This method was used in Good et al. (2013) to find the response to RCP sce-
 467 narios using the forcing computed by F13. They use this to simulate only differences be-
 468 tween RCP scenarios, while we attempt to simulate the full temperature evolution since
 469 the historical runs started until year 2100. Another difference to our approach is that
 470 we obtain a smoother estimate of the expected response to forcing, with fluctuations only
 471 coming from the forcing, while the responses of Good et al. (2013) are themselves influ-
 472 enced by internal variability.

473 Larson and Portmann (2016) note that the non-parametric model written in mat-
 474 rix form: $\mathbf{Y} = \mathbf{X}\Delta\mathbf{F}/F_0$ can be inverted to estimate the forcing increments $\Delta\mathbf{F}$, which
 475 can further be summed up to find the forcing time series. In this equation \mathbf{Y} is a vec-
 476 tor of the time evolution of a climate variable, and \mathbf{X} is a matrix containing the same
 477 variable in the abrupt4xCO₂ experiment. Their resulting forcing estimate depends also
 478 on the forcing estimate F_0 from the abrupt4xCO₂ experiment, which introduces a po-

479 tential source of bias in the estimate. Internal variability from \mathbf{X} and \mathbf{Y} can lead to a
 480 very noisy estimate, but some of this is removed when they replace the original abrupt4xCO₂
 481 time series with a fitted exponential response. With our method we also greatly reduce
 482 the influence of internal variability from the experiment where the forcing is to be es-
 483 timated by smoothing it with our linear response to the estimated forcing. So we can
 484 say that there is a trade-off between a noisy estimate and having more parameters to be
 485 estimated. The method by Larson and Portmann (2016) is treated as an alternative to
 486 the F13 method, but here we show how the F13 method and the linear response can be
 487 put into one framework. While Larson and Portmann (2016) can demonstrate that their
 488 method is not directly dependent of a changing feedback parameter, our method also has
 489 the power to explain why this can be the case.

490 5 Conclusions

491 The method presented here cleanly separates between forcing and responses to forc-
 492 ing, where the estimated parameters from abrupt4xCO₂ experiments are used to deter-
 493 mine forcing and surface temperature responses for other experiments. The resulting RCP
 494 forcing estimates at the end of the 21st century is closer to the target levels than pre-
 495 vious estimates by F13. Our high forcing estimates are strongly influenced by the high
 496 magnitude of the feedback parameter λ_1 at annual time scales. Unfortunately this value
 497 is uncertain, as it depends crucially on the first few years of adjustment. Using more en-
 498 semble members of abrupt4xCO₂ experiments may help constrain the estimate of λ_1 (M. Ru-
 499 genstein, Gregory, et al., 2016). More members would also constrain regression estimates
 500 of forcing in general (Forster et al., 2016).

501 Forcing based on fixed-SST methods is often higher than the regression estimate
 502 over 150 years (Andrews et al., 2012; Tang et al., 2019), has a smaller uncertainty and
 503 is more computationally efficient (Forster et al., 2016). However, these forcing estimates
 504 are only available for a few models and scenarios in CMIP5. They will be available for
 505 more models and scenarios in CMIP6 (Smith et al., 2020), but far from all. The forc-
 506 ing estimation method presented here could therefore be a valuable supplement in the
 507 cases where fixed-SST forcing is unknown, particularly for models where a linear rela-
 508 tion between N and T is a poor approximation. Improved forcing estimates could help
 509 to quantify the dependency of forcing value on CO₂ concentration in studies compar-
 510 ing e.g. 0.5x, 2x, 4x, 8x CO₂, and temperature dependence of feedbacks (Bloch-Johnson
 511 et al., 2021).

512 Putting forcing, linear responses, and nonconstancy of the global feedback param-
 513 eter into a unified framework provides also an important insight into why the traditional
 514 regression-based forcing estimates may be too low. Furthermore, it suggests how these
 515 methods can be improved to provide better forcing estimates, resolving the problems caused
 516 by assuming a constant feedback parameter in regression-based methods (Forster et al.,
 517 2016).

518 Acknowledgments

519 The CMIP5 data are available at <https://esgf-node.llnl.gov/projects/cmip5/>. The
 520 forcing estimates from this paper will be stored in <https://dataverse.no/>, and can be
 521 accessed through <https://doi.org/10.18710/IHUVTB>. Our python code will be per-
 522 manently stored in zenodo (link will be inserted when paper is accepted. The code is cur-
 523 rently available at <https://github.com/Hegebf/CMIP5-forcing>). We thank Timothy
 524 Andrews and an anonymous reviewer for helpful suggestions improving our manuscript.

525 References

526 Andrews, T., Gregory, J. M., & Webb, M. J. (2015). The Dependence of Ra-

- 527 radiative Forcing and Feedback on Evolving Patterns of Surface Tempera-
 528 ture Change in Climate Models. *Journal of Climate*, 28(4), 1630–1648.
 529 <https://doi.org/10.1175/JCLI-D-14-00545.1>
- 530 Andrews, T., Gregory, J. M., Webb, M. J., & Taylor, K. E. (2012). Forc-
 531 ing, feedbacks and climate sensitivity in CMIP5 coupled atmosphere-
 532 ocean climate models. *Geophysical Research Letters*, 39, L09712.
 533 <https://doi.org/10.1029/2012GL051607>
- 534 Andrews, T., Smith, C. J., Myhre, G., Forster, P. M., Chadwick, R., & Ackerley, D.
 535 (2021). Effective Radiative Forcing in a GCM With Fixed Surface Tempera-
 536 tures. *Journal of Geophysical Research: Atmospheres*, 126, e2020JD033880.
 537 <https://doi.org/10.1029/2020JD033880>
- 538 Andrews, T., & Webb, M. J. (2018). The Dependence of Global Cloud and Lapse
 539 Rate Feedbacks on the Spatial Structure of Tropical Pacific Warming. *Journal*
 540 *of Climate*, 31(2), 641–654. <https://doi.org/10.1175/JCLI-D-17-0087.1>
- 541 Armour, K. C. (2017). Energy budget constraints on climate sensitivity in light
 542 of inconstant climate feedbacks. *Nature Climate Change*, 7, 331 – 335.
 543 <https://doi.org/10.1038/nclimate3278>
- 544 Armour, K. C., Bitz, C. M., & Roe, G. H. (2013). Time-Varying Climate Sen-
 545 sitivity from Regional Feedbacks. *Journal of Climate*, 26, 4518–4534.
 546 <https://doi.org/10.1175/JCLI-D-12-00544.1>
- 547 Bacmeister, J. T., Hannay, C., Medeiros, B., Gettelman, A., Neale, R., Fredriksen,
 548 H. B., ... Otto-Bliesner, B. (2020). CO2 increase experiments using the Com-
 549 munity Earth System Model (CESM): Relationship to climate sensitivity and
 550 comparison of CESM1 to CESM2. *Journal of Advances in Modeling Earth*
 551 *Systems*, 12, e2020MS002120. <https://doi.org/10.1029/2020MS002120>
- 552 Bloch-Johnson, J., Rugenstein, M., & Abbot, D. S. (2020). Spatial radiative feed-
 553 backs from internal variability using multiple regression. *Journal of Climate*,
 554 33, 4121–4140. <https://doi.org/10.1175/JCLI-D-19-0396.1>
- 555 Bloch-Johnson, J., Rugenstein, M., Stolpe, M. B., Rohrschneider, T., Zheng, Y., &
 556 Gregory, J. M. (2021). Climate Sensitivity Increases Under Higher CO₂ Levels
 557 Due to Feedback Temperature Dependence. *Geophysical Research Letters*, 48,
 558 e2020GL089074. <https://doi.org/10.1029/2020GL089074>
- 559 Byrne, B., & Goldblatt, C. (2014). Radiative forcing at high concentrations of
 560 well-mixed greenhouse gases. *Geophysical Research Letters*, 41, 152–160.
 561 <https://doi.org/10.1002/2013GL058456>
- 562 Ceppi, P., & Gregory, J. M. (2017). Relationship of tropospheric stabil-
 563 ity to climate sensitivity and Earth’s observed radiation budget. *Pro-*
 564 *ceedings of the National Academy of Sciences*, 114(50), 13126–13131.
 565 <https://doi.org/10.1073/pnas.1714308114>
- 566 Chung, E.-S., & Soden, B. J. (2015). An assessment of methods for computing
 567 radiative forcing in climate models. *Environmental Research Letters*, 10(7),
 568 074004. <https://doi.org/10.1088/1748-9326/10/7/074004>
- 569 Colman, R. A., & Hanson, L. I. (2013). On atmospheric radiative feedbacks asso-
 570 ciated with climate variability and change. *Climate Dynamics*, 40(1), 475–492.
 571 <https://doi.org/10.1007/s00382-012-1391-3>
- 572 Colman, R. A., & Power, S. B. (2010). Atmospheric radiative feedbacks associated
 573 with transient climate change and climate variability. *Climate Dynamics*, 34,
 574 919–933. <https://doi.org/10.1007/s00382-009-0541-8>
- 575 Dessler, A. E. (2020). Potential Problems Measuring Climate Sensitiv-
 576 ity from the Historical Record. *Journal of Climate*, 33(6), 2237–2248.
 577 <https://doi.org/10.1175/JCLI-D-19-0476.1>
- 578 Dessler, A. E., & Forster, P. M. (2018). An Estimate of Equilibrium Climate Sen-
 579 sitivity From Interannual Variability. *Journal of Geophysical Research: Atmo-*
 580 *spheres*, 123(16), 8634–8645. <https://doi.org/10.1029/2018JD028481>
- 581 Dong, Y., Armour, K. C., Zelinka, M. D., Proistosescu, C., Battisti, D. S., Zhou,

- 582 C., & Andrews, T. (2020). Intermodel Spread in the Pattern Effect and Its
 583 Contribution to Climate Sensitivity in CMIP5 and CMIP6 Models. *Journal of*
 584 *Climate*, *33*(18), 7755–7775. <https://doi.org/10.1175/JCLI-D-19-1011.1>
- 585 Dong, Y., Proistosescu, C., Armour, K. C., & Battisti, D. S. (2019). Attributing
 586 Historical and Future Evolution of Radiative Feedbacks to Regional Warming
 587 Patterns using a Green’s Function Approach: The Preeminence of the Western
 588 Pacific. *Journal of Climate*, *32*(17), 5471–5491. <https://doi.org/10.1175/JCLI-D-18-0843.1>
- 589 Edwards, C., & Penney, D. (2007). *Differential equations and boundary value prob-*
 590 *lems: Computing and modelling (Fourth edition)*. Pearson.
- 591 Etminan, M., Myhre, G., Highwood, E. J., & Shine, K. P. (2016). Radiative forc-
 592 ing of carbon dioxide, methane, and nitrous oxide: A significant revision of
 593 the methane radiative forcing. *Geophysical Research Letters*, *43*(24), 12,614–
 594 12,623. <https://doi.org/10.1002/2016GL071930>
- 595 Forster, P. M., Andrews, T., Good, P., Gregory, J. M., Jackson, L. S., & Zelinka, M.
 596 (2013). Evaluating adjusted forcing and model spread for historical and future
 597 scenarios in the CMIP5 generation of climate models. *Journal of Geophysical*
 598 *Research*, *118*, 1139–1150. <https://doi.org/10.1002/jgrd.50174>
- 599 Forster, P. M., Richardson, T., Maycock, A. C., Smith, C. J., Samset, B. H., Myhre,
 600 G., ... Schulz, M. (2016). Recommendations for diagnosing effective radiative
 601 forcing from climate models for CMIP6. *Journal of Geophysical Research:*
 602 *Atmospheres*, *121*(20), 12,460–12,475. <https://doi.org/10.1002/2016JD025320>
- 603 Fredriksen, H.-B., & Rypdal, M. (2017). Long-range persistence in global surface
 604 temperatures explained by linear multibox energy balance models. *Journal of*
 605 *Climate*, *30*, 7157–7168. <https://doi.org/10.1175/JCLI-D-16-0877.1>
- 606 Geoffroy, O., Saint-Martin, D., Bellon, G., Voldoire, A., Olivié, D., & Tytéca,
 607 S. (2013). Transient Climate Response in a Two-Layer Energy-Balance
 608 Model. Part II: Representation of the Efficacy of Deep-Ocean Heat Uptake
 609 and Validation for CMIP5 AOGCMs. *Journal of Climate*, *26*(6), 1859–1876.
 610 <https://doi.org/10.1175/JCLI-D-12-00196.1>
- 611 Geoffroy, O., Saint-Martin, D., Olivié, D. J. L., Voldoire, A., Bellon, G., &
 612 Tytéca, S. (2013). Transient Climate Response in a Two-Layer Energy-
 613 Balance Model. Part I: Analytical Solution and Parameter Calibration Us-
 614 ing CMIP5 AOGCM Experiments. *Journal of Climate*, *26*, 1841–1857.
 615 <https://doi.org/10.1175/JCLI-D-12-00195.1>
- 616 Good, P., Gregory, J. M., & Lowe, J. A. (2011). A step-response simple climate
 617 model to reconstruct and interpret AOGCM projections. *Geophysical Research*
 618 *Letters*, *38*, L01703. <https://doi.org/10.1029/2010GL045208>
- 619 Good, P., Gregory, J. M., Lowe, J. A., & Andrews, T. (2013). Abrupt CO₂ ex-
 620 periments as tools for predicting and understanding CMIP5 representative
 621 concentration pathway projections. *Climate Dynamics*, *40*(3), 1041–1053.
 622 <https://doi.org/10.1007/s00382-012-1410-4>
- 623 Gregory, J. M., & Andrews, T. (2016). Variation in climate sensitivity and feedback
 624 parameters during the historical period. *Geophysical Research Letters*, *43*(8),
 625 3911–3920. <https://doi.org/10.1002/2016GL068406>
- 626 Gregory, J. M., Andrews, T., & Good, P. (2015). The inconstancy of the transient
 627 climate response parameter under increasing CO₂. *Philosophical Transactions*
 628 *of the Royal Society A: Mathematical, Physical and Engineering Sciences*, *373*,
 629 20140417. <https://doi.org/10.1098/rsta.2014.0417>
- 630 Gregory, J. M., Ingram, W. J., Palmer, M. A., Jones, G. S., Stott, P. A., Thorpe,
 631 R. B., ... Williams, K. D. (2004). A new method for diagnosing radiative
 632 forcing and climate sensitivity. *Geophysical Research Letters*, *31*, L03205.
 633 <https://doi.org/10.1029/2003GL018747>
- 634 Hansen, J., Sato, M., Ruedy, R., Nazarenko, L., Lacis, A., Schmidt, G. A., ...
 635 Zhang, S. (2005). Efficacy of climate forcings. *Journal of Geophysical Re-*
 636

- 637 *search: Atmospheres*, 110(D18). <https://doi.org/10.1029/2005JD005776>
- 638 Hasselmann, K., Sausen, R., Maier-Reimer, E., & Voss, R. (1993). On the cold start
639 problem in transient simulations with coupled atmosphere-ocean models. *Cli-*
640 *mate Dynamics*, 9(6), 53–61. <https://doi.org/10.1007/BF00210008>
- 641 Held, I., Winton, M., Takahashi, K., Delworth, T. L., Zeng, F., & Vallis, G. (2010).
642 Probing the Fast and Slow Components of Global Warming by Returning
643 Abruptly to Preindustrial Forcing. *Journal of Climate*, 23, 2418 – 2427.
644 <https://doi.org/10.1175/2009JCLI3466.1>
- 645 Kay, J. E., Deser, C., Phillips, A., Mai, A., Hannay, C., Strand, G., . . . Vertenstein,
646 M. (2015). The Community Earth System Model (CESM) Large Ensemble
647 Project: A Community Resource for Studying Climate Change in the Pres-
648 ence of Internal Climate Variability. *Bulletin of the American Meteorological*
649 *Society*, 96(8), 1333-1349. <https://doi.org/10.1175/BAMS-D-13-00255.1>
- 650 Larson, E. J. L., & Portmann, R. W. (2016). A Temporal Kernel Method to Com-
651 pute Effective Radiative Forcing in CMIP5 Transient Simulations. *Journal of*
652 *Climate*, 29(4), 1497-1509. <https://doi.org/10.1175/JCLI-D-15-0577.1>
- 653 Loeb, N. G., Wang, H., Allan, R. P., Andrews, T., Armour, K., Cole, J. N. S.,
654 . . . Wyser, K. (2020). New generation of climate models track
655 recent unprecedented changes in earth’s radiation budget observed
656 by ceres. *Geophysical Research Letters*, 47(5), e2019GL086705.
657 <https://doi.org/10.1029/2019GL086705>
- 658 Lutsko, N. J., & Takahashi, K. (2018). What Can the Internal Variability of CMIP5
659 Models Tell Us about Their Climate Sensitivity? *Journal of Climate*, 31(13),
660 5051-5069. <https://doi.org/10.1175/JCLI-D-17-0736.1>
- 661 Marvel, K., Pincus, R., Schmidt, G. A., & Miller, R. L. (2018). Internal
662 Variability and Disequilibrium Confound Estimates of Climate Sensitiv-
663 ity From Observations. *Geophysical Research Letters*, 45(3), 1595-1601.
664 <https://doi.org/10.1002/2017GL076468>
- 665 Menzel, M. E., & Merlis, T. M. (2019). Connecting Direct Effects of CO2 Radiative
666 Forcing to Ocean Heat Uptake and Circulation. *Journal of Advances in Model-*
667 *ing Earth Systems*, 11(7), 2163-2176. <https://doi.org/10.1029/2018MS001544>
- 668 Meraner, K., Mauritsen, T., & Voigt, A. (2013). Robust increase in equilibrium cli-
669 mate sensitivity under global warming. *Geophysical Research Letters*, 40(22),
670 5944–5948. <https://doi.org/10.1002/2013GL058118>
- 671 Myhre, G., Highwood, E. J., Shine, K. P., & Stordal, F. (1998). New estimates of ra-
672 diative forcing due to well mixed greenhouse gases. *Geophysical Research Let-*
673 *ters*, 25(14), 2715–2718. <https://doi.org/10.1029/98GL01908>
- 674 Olonscheck, D., Rugenstein, M., & Marotzke, J. (2020). Broad consis-
675 tency between observed and simulated trends in sea surface tempera-
676 ture patterns. *Geophysical Research Letters*, 47(10), e2019GL086773.
677 <https://doi.org/10.1029/2019GL086773>
- 678 Paynter, D., & Frölicher, T. L. (2015). Sensitivity of radiative forcing, ocean heat
679 uptake, and climate feedback to changes in anthropogenic greenhouse gases
680 and aerosols. *Journal of Geophysical Research: Atmospheres*, 120(19), 9837–
681 9854. <https://doi.org/10.1002/2015JD023364>
- 682 Pincus, R., Forster, P. M., & Stevens, B. (2016). The Radiative Forcing Model
683 Intercomparison Project (RFMIP): experimental protocol for CMIP6. *Geosci-*
684 *entific Model Development*, 9(9), 3447–3460. [https://doi.org/10.5194/gmd-9-](https://doi.org/10.5194/gmd-9-3447-2016)
685 [3447-2016](https://doi.org/10.5194/gmd-9-3447-2016)
- 686 Proistosescu, C., & Huybers, P. J. (2017). Slow climate mode reconciles histor-
687 ical and model-based estimates of climate sensitivity. *Sciences Advances*, 3,
688 e1602821. <https://doi.org/10.1126/sciadv.1602821>
- 689 Richardson, T. B., Forster, P. M., Smith, C. J., Maycock, A. C., Wood, T., An-
690 drews, T., . . . Watson-Parris, D. (2019). Efficacy of Climate Forcings in
691 PDRMIP Models. *Journal of Geophysical Research: Atmospheres*, 124(23),

- 12824-12844. <https://doi.org/10.1029/2019JD030581>
- 692 Rohrschneider, T., Stevens, B., & Mauritsen, T. (2019). On simple representations
693 of the climate response to external radiative forcing. *Climate Dynamics*, *53*(5),
694 3131–3145. <https://doi.org/10.1007/s00382-019-04686-4>
- 695 Rugestein, M., Bloch-Johnson, J., Gregory, J., Andrews, T., Mauritsen, T., Li, C.,
696 ... Knutti, R. (2020). Equilibrium Climate Sensitivity Estimated by Equili-
697 brating Climate Models. *Geophysical Research Letters*, *47*(4), e2019GL083898.
698 <https://doi.org/10.1029/2019GL083898>
- 699 Rugestein, M., Caldeira, K., & Knutti, R. (2016). Dependence of global radiative
700 feedbacks on evolving patterns of surface heat fluxes. *Geophysical Research*
701 *Letters*, *43*(18), 9877–9885. <https://doi.org/10.1002/2016GL070907>
- 702 Rugestein, M., Gregory, J. M., Schaller, N., Sedláček, J., & Knutti, R. (2016). Mul-
703 tiannual Ocean–Atmosphere Adjustments to Radiative Forcing. *Journal of Cli-*
704 *mate*, *29*(15), 5643–5659. <https://doi.org/10.1175/JCLI-D-16-0312.1>
- 705 Rugestein, M. A. A., & Armour, K. C. (2021). Three Flavors of Radia-
706 tive Feedbacks and Their Implications for Estimating Equilibrium Cli-
707 mate Sensitivity. *Geophysical Research Letters*, *48*(15), e2021GL092983.
708 <https://doi.org/10.1029/2021GL092983>
- 709 Rypdal, M., & Rypdal, K. (2014). Long-Memory Effects in Linear Response Models
710 of Earth’s Temperature and Implications for Future Global Warming. *Journal*
711 *of Climate*, *27*, 5240–5258. <https://doi.org/10.1175/JCLI-D-13-00296.1>
- 712 Sherwood, S. C., Bony, S., Boucher, O., Bretherton, C., Forster, P. M., Gregory,
713 J. M., & Stevens, B. (2015). Adjustments in the Forcing-Feedback Framework
714 for Understanding Climate Change. *Bulletin of the American Meteorological*
715 *Society*, *96*(2), 217–228. <https://doi.org/10.1175/BAMS-D-13-00167.1>
- 716 Smith, C. J., Kramer, R. J., Myhre, G., Alterskjær, K., Collins, W., Sima, A.,
717 ... Forster, P. M. (2020). Effective radiative forcing and adjustments in
718 cmip6 models. *Atmospheric Chemistry and Physics*, *20*(16), 9591–9618.
719 <https://doi.org/10.5194/acp-20-9591-2020>
- 720 Smith, C. J., Kramer, R. J., Myhre, G., Forster, P. M., Soden, B. J., Andrews, T.,
721 ... Watson-Parris, D. (2018). Understanding Rapid Adjustments to Di-
722 verse Forcing Agents. *Geophysical Research Letters*, *45*(21), 12,023–12,031.
723 <https://doi.org/10.1029/2018GL079826>
- 724 Soden, B. J., Collins, W. D., & Feldman, D. R. (2018). Reducing
725 uncertainties in climate models. *Science*, *361*(6400), 326–327.
726 <https://doi.org/10.1126/science.aau1864>
- 727 Tang, T., Shindell, D., Faluvegi, G., Myhre, G., Olivié, D., Voulgarakis, A., ...
728 Smith, C. (2019). Comparison of Effective Radiative Forcing Calculations Us-
729 ing Multiple Methods, Drivers, and Models. *Journal of Geophysical Research:*
730 *Atmospheres*, *124*(8), 4382–4394. <https://doi.org/10.1029/2018JD030188>
- 731 Trossman, D. S., Palter, J. B., Merlis, T. M., Huang, Y., & Xia, Y. (2016).
732 Large-scale ocean circulation-cloud interactions reduce the pace of tran-
733 sient climate change. *Geophysical Research Letters*, *43*(8), 3935–3943.
734 <https://doi.org/10.1002/2016GL067931>
- 735 van Vuuren, D. P., Edmonds, J., Kainuma, M., Riahi, K., Thomson, A., Hibbard,
736 K., ... Rose, S. K. (2011). The representative concentration pathways: an
737 overview. *Climatic Change*, *109*, 5–31. [https://doi.org/10.1007/s10584-011-](https://doi.org/10.1007/s10584-011-0148-z)
738 [0148-z](https://doi.org/10.1007/s10584-011-0148-z)
- 739 Williams, K. D., Ingram, W. J., & Gregory, J. M. (2008). Time Variation of Ef-
740 fective Climate Sensitivity in GCMs. *Journal of Climate*, *21*(19), 5076–5090.
741 <https://doi.org/10.1175/2008JCLI2371.1>
- 742 Winton, M., Takahashi, K., & Held, I. M. (2010). Importance of Ocean Heat Uptake
743 Efficacy to Transient Climate Change. *Journal of Climate*, *23*(9), 2333–2344.
744 <https://doi.org/10.1175/2009JCLI3139.1>
- 745 Zelinka, M. D., Klein, S. A., Taylor, K. E., Andrews, T., Webb, M. J., Gregory,
746

- 747 J. M., & Forster, P. M. (2013). Contributions of Different Cloud Types to
748 Feedbacks and Rapid Adjustments in CMIP5. *Journal of Climate*, *26*(14),
749 5007–5027. <https://doi.org/10.1175/JCLI-D-12-00555.1>
- 750 Zelinka, M. D., Myers, T. A., McCoy, D. T., Po-Chedley, S., Caldwell, P. M.,
751 Ceppi, P., . . . Taylor, K. E. (2020). Causes of Higher Climate Sensitivity
752 in CMIP6 Models. *Geophysical Research Letters*, *47*(1), e2019GL085782.
753 <https://doi.org/10.1029/2019GL085782>
- 754 Zhou, C., Zelinka, M. D., Dessler, A. E., & Klein, S. A. (2015). The relationship
755 between interannual and long-term cloud feedbacks. *Geophysical Research Let-*
756 *ters*, *42*(23), 10,463–10,469. <https://doi.org/10.1002/2015GL066698>
- 757 Zhou, C., Zelinka, M. D., & Klein, S. A. (2016). Impact of decadal cloud vari-
758 ations on the Earth’s energy budget. *Nature Geoscience*, *9*(12), 871–874.
759 <https://doi.org/10.1038/ngeo2828>